Aalborg Universitet

Thermal Analysis of Multilevel Grid-side Converters for 10-MW Wind turbines under Low-Voltage Ride Through

Ma, Ke; Blaabjerg, Frede; Liserre, Marco

Thermal Analysis of Multilevel Grid-side Converters for 10-MW Wind turbines under Low-Voltage Ride Through

Ke Ma
Frede Blaabjerg
Marco Liserre

Suggested Citation

Thermal Analysis of Multilevel Grid Side Converters for 10 MW Wind Turbines under Low Voltage Ride Through

K. Ma[1], F. Blaabjerg[1], M. Liserre[2]

[1] Department of Energy Technology, Aalborg University
Pontoppidanstraede 101, DK-9220 Aalborg East, Denmark
kema@et.aau.dk, fbl@et.aau.dk

[2] Dept of Electrotechnical and Electronic Engineering, Polytechnic of Bari
Via E.Orabona 4, 70125 - Bari, Italy
liserre@poliba.it

Abstract – As the power level of a single wind turbine is continuously pushed up-even to 7 MW, the wind power generation systems are required to be more reliable, and able to withstand extreme grid disturbances. Moreover, it is becoming a need that the wind power generation system should be more active in the power network, and able to contribute to the grid recovery by injecting reactive current during grid faults. Consequently, the full-scale power converter solutions are becoming more and more popular to fulfill the growing challenges in the wind power application. Nevertheless, the loading of the power devices in full-scale power converters, especially during grid faults, may compromise the reliability performance and further increase the cost of the system. In this paper, three promising grid side multilevel converter topologies for the next generation 10 MW wind turbines are proposed and basically designed as case study. The operation status, as well as the reliability related performances are investigated aimed at various Low Voltage Ride Through (LVRT) conditions. It is found that all of the proposed converter topologies will suffer from higher junction temperature in some heavily loaded power devices (especially the diodes) under LVRT operation. And the three-level and five-level H-bridge topologies show more potential to reduce the inequality and level of device stress than the well-known three-level Neutral Point Clamped topology.

Index Terms – Wind power generation, Multilevel converter, LVRT, Thermal analysis.

I. INTRODUCTION

The European Union is committed to source 20 % of its energy from renewables by 2020 [1]. As the most promising candidate, the wind energy production integrated into the power grid is booming up all over the world. Meanwhile, the power capacity of a single wind turbine is increasing continuously to reduce the price pr. produced kWh, as the cutting-edge achievement, 7 MW offshore wind turbines have already been presented on the market [2]-[4]. Consequently, due to much more significant impact to the power grid after a failure or disconnection than ever before, the wind power generation system is required to be more reliable and able to withstand some extreme grid disturbances. The Transmission System Operators (TSO) have issued stricter Low Voltage Ride Through (LVRT) grid codes, as shown in Fig. 1 [5] for

different countries, in which the boundaries with various voltage dips as well as their allowable disturbance time are defined. Moreover, it is becoming a need that the wind power generation system should also provide reactive current (up to 100% rated current capacity of converter) to contribute to the grid recovery, when LVRT is present, as shown in Fig. 2 where the required amount of reactive current with relation to the grid voltage is indicated by German grid codes [6].
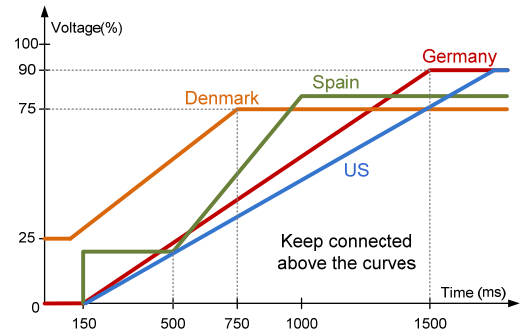
Fig. 1. Grid codes of wind turbines under low voltage ride through by different countries [5].
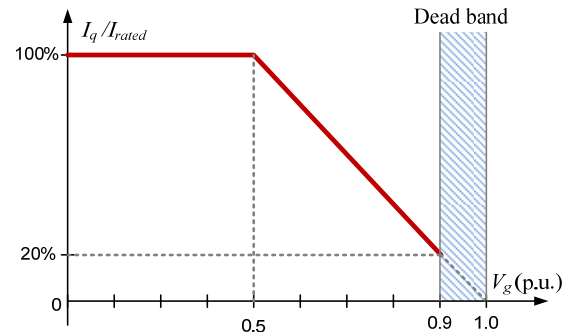
Fig. 2. Reactive current requirements vs. grid voltage V_g during low voltage ride through [6].

The stricter grid codes as well as the higher reliability requirements push the solutions of wind power generation system moving from Doubly Fed Induction Generator (DFIG) with partial-rated power converter to Permanent Magnet Synchronous Generator (PMSG) with full-scale power converter. Lots of work has been done related to how to control the wind power converter to satisfy the grid codes

during LVRT [7], [8]. However, the loss and thermal performance under this condition, especially when using MW full-scale power converters, are another important and interesting topics needed for further investigations. The extreme loading of the power devices under grid disturbances could result in de-rerated converter power, cost-ineffective power semiconductors, complicated heat sink system, as well as reduced reliability of the converter.

In this paper, three promising grid-side multilevel converters for 10 MW wind turbines are proposed and basically designed. The evaluation criteria will mainly aim at the utilization and thermal performances of power switching devices during various LVRT conditions. Studies regarding the converter output, as well as loss and thermal distributions under different grid voltage dips/wind speeds are presented and compared.

II. PROMISING TOPOLOGIES AND BASIC DESIGN

The concept and major parts of a variable speed wind turbine with full-scale power converter are shown in Fig. 3.

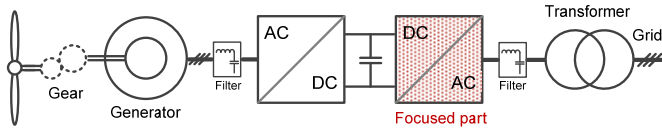Fig. 3. Wind power generation system with full scale converter.

As mentioned before, the power capacity of a single wind turbine keeps climbing up even to 7 MW, and medium voltage (1 kV-10 kV) would be interesting and needed to reduce the current rating in the wirings and switching devices under such a high power level. It is more and more difficult for the traditional two-level voltage source converter to achieve acceptable performance with the available switching devices [9]. With the abilities of more output voltage levels, higher voltage amplitude and larger output power, multilevel converter topologies are becoming the most promising candidates in the application of full-scale power/medium-voltage wind power conversion [9]-[13].

Because the grid side converter in Fig. 3 is directly interfaced with the power grid, and plays a key role to comply with the stricter standards during grid faults, the discussions will mainly focus on this part of the generation system. More detailed information about the generator side AC/DC converter is included in [9] and will not be discussed in this paper. Among various multilevel topologies, three of them are of interest:

As one of the most commercialized multilevel converters on the market, three-level neutral point diode clamped topology (3L-NPC) is shown in Fig. 4. The mid-point potential fluctuation of the DC bus is a main drawback, but this problem has been extensively researched and is considered improved [10]. However, it is found that the loss distribution between the outer and the inner power devices in

a switching arm is unequal, and this problem may lead to cost-ineffective power device utilization, when it is practically designed [10], [13].

The three-level H-bridge topology (3L-HB) could be another choice in the wind power application, as shown in Fig. 5. The clamped diodes in 3L-NPC solution are eliminated [13], and only half of the DC bus voltage is needed without mid-point, the cost for DC link capacitors can be thereby reduced. However, extra length, loss and inductance in the cables as well as the cost will be a major drawback. Also zero-sequence current path is introduced in this configuration, where special components or control methods are needed to block the zero-sequence current [14].
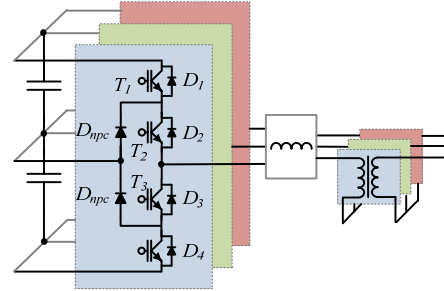
Fig. 4. Three-level Neutral-Point-Clamped converter topology (3L-NPC).
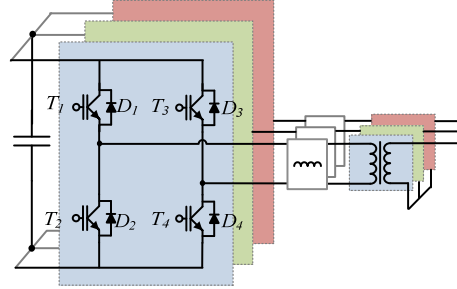
Fig. 5. Three-level H-bridge converter topology (3L-HB).
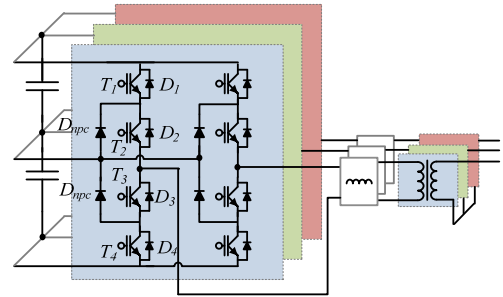
Fig. 6. Five-level H-bridge converter topology (5L-HB).

Another promising converter configuration (5L-HB) which makes use of the switching arms of 3L-NPC topology, and the H-bridge structure of the 3L-HB topology, is shown in Fig. 6. It shares the same special requirements for open-winding transformer as 3L-HB topology. With switching devices of the same voltage rating, this converter can achieve five-level voltage output and doubled voltage amplitude

compared to the 3L-NPC and 3L-HB solution. These features enable less current rating in the switching devices as well as the cables [15]. However, the 5L-HB topology introduces more power devices/cables as well as zero-sequence current path, all of which could increase the cost of the converter system.

The basic design of each converter topology for a case study is as follows: All of the power switching devices have the commutated voltage of 2.8 kV in order to utilize the available and dominant 4.5 kV high-power IGCT/IGBT on the market, then the DC bus and maximum output voltage of each configuration can be determined. The most commonly used carrier based PWM method for each converter topology is applied and the equivalent switching frequency is typically designed to be 800 Hz in order to get an acceptable switching loss in the power devices. The output filter inductance is designed to limit the maximum current ripple to 25% of the rated current amplitude, and the filter capacitance is not taken into account. The power control method can be found in [13], the references of active and reactive current delivered by the inverter under different voltage dips is selected according to the German grid codes which is shown in Fig. 2 [6]. The design parameters are summarized in Table I. For simplicity of analysis, the power grid is considered as three ideal AC voltage sources, and the transformers are assumed ideal. The DC bus voltage during LVRT is assumed to be controlled at 110% of the rated value by a DC bus chopper, which is a typical industrial solution used to absorb the active power from the generator. The detailed loss and efficiency performances of each topology under normal grid operation can be found in [11].

Table I. Parameters of different converter topologies for case study.

Configurations	3L-NPC	3L-HB	5L-HB
Rated active power	10 MW		
Equivalent sw. freq.	800 Hz		
Modulation method	PD-PWM	Unipolar-PWM	POD-PWM
DC bus voltage	5.6 kV	2.8 kV	5.6 kV
Primary side voltage*	1.9 kV rms	1.9 kV rms	3.8 kV rms
Rated phase current	1.75 kA rms	1.75 kA rms	972 A rms
Filter inductance	1.13 mH (0.2 p.u.)	1.13 mH (0.2 p.u.)	2.89 mH (0.12 p.u.)

* Rated phase voltage in the primary windings of transformer.

III. OPERATION STATUS UNDER BALANCED LVRT

After the parameters for each converter topology are settled, the operation status with the information of output voltage, load current and delivered power under various LVRT conditions can be derived and simulated. In order to facilitate the investigation and demonstration of the converter operation characteristics under LVRT, three-phase balanced grid faults are first taken into account.

Fig. 7 summarizes the active/ reactive power delivered by the grid side converter under various balanced grid voltage dips of three-phases. Because the injected reactive current under LVRT is defined by grid codes in Fig. 2, the reactive power Q delivered by the converter is only decided by the grid voltage. However, there is still some flexibility to adjust the active current when the grid voltage is above 0.5 p.u.. In order to reduce the stress of braking chopper on DC bus and maintain the DC bus voltage [7], [8], the active power P delivered by the converter under grid voltage above 0.5 p.u. should refer to the generated power by wind turbines. Worst condition is assumed when the generation system is set to provide as much active power as possible, and the pitch control of wind turbine does not have enough time to activate [7], [8]. The situations of 12 m/s wind speed (10 MW generated power), 10 m/s (6.3 MW generated power) and 8 m/s (3.2 MW generated power) [16], [17] are indicated respectively in Fig. 7.
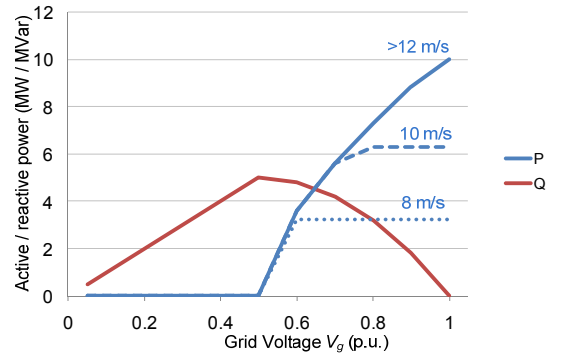

Fig. 7. Active and reactive power delivered by converter during balanced LVRT (based on German grid codes in Fig. 2).
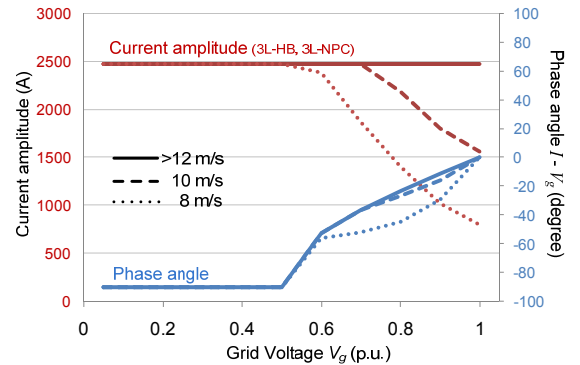
Fig. 8. Amplitude and phase angle of load current during balanced LVRT (based on German grid codes in Fig. 2, the 5L-HB converter has half current amplitude).

The current amplitude and phase angle (between load current and grid voltage) under three-phase balanced LVRT are shown in Fig. 8, in which the situation of different wind speeds at 12 m/s, 10 m/s and 8 m/s are indicated respectively. It can be seen that when the grid voltage is below 0.5 p.u., both of the current amplitude and phase angle keep constant because of 100% rated reactive current injection, however when the grid voltage is above 0.5 p.u., the current amplitude and phase angle dramatically change with the variation of grid voltage and wind speed.

Fig. 9. Simulation outputs when LVRT is presented (normal operation: v_w=10 m/s, P_G=6.3 MW / LVRT: V_g=0.05 p.u., $I_{reactive}$=100% I_{rated}), output voltage pulses (Green), grid voltage (blue), phase current (red).
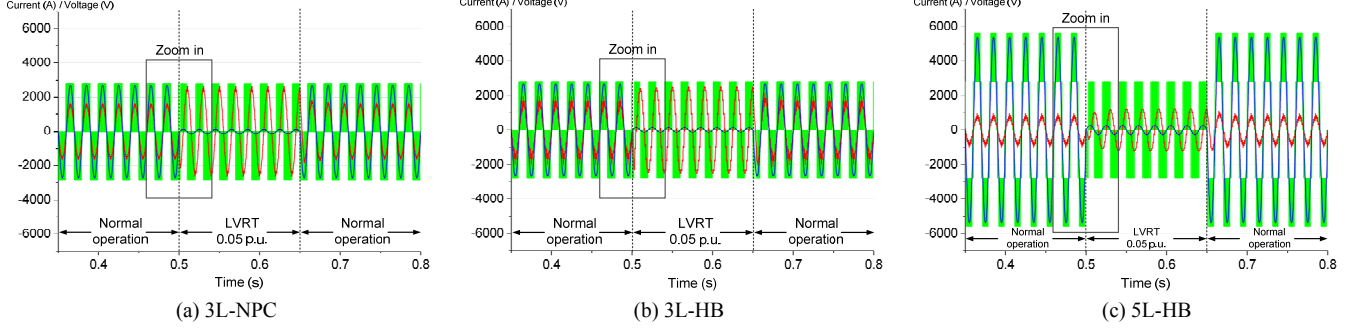

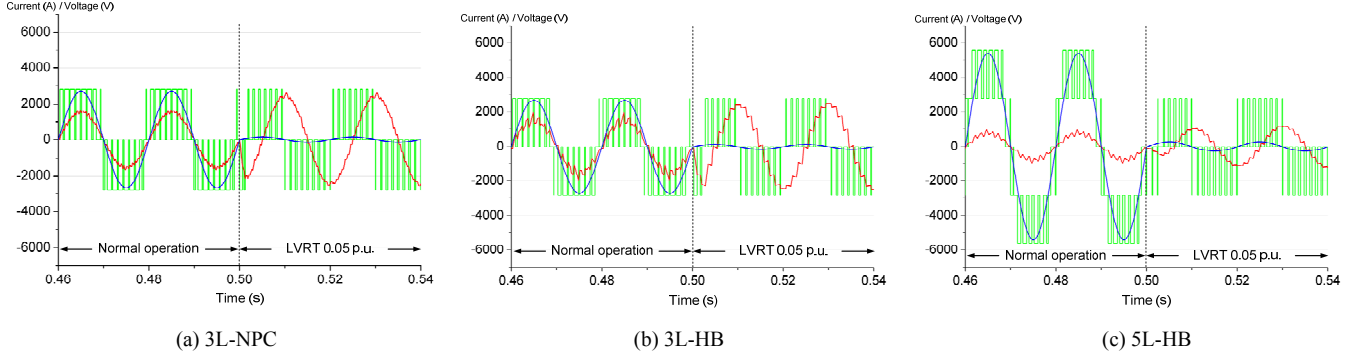Fig.10. Zoom in area of Fig. 9, output voltage pulses (Green), grid voltage (blue), phase current (red).
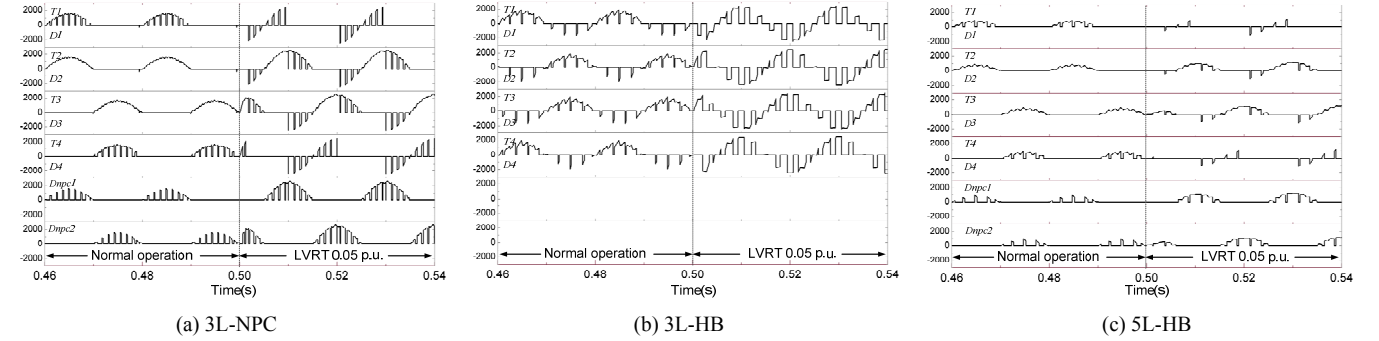

Fig. 11. Current distribution in the power devices of Fig. 10.

The simulations are carried out based on PLECS Blockset in Simulink [21], and the simulation parameters are consistent with the ones in Table I. A normal operation status of each converter is first assumed at wind speed of 10 m/s, which is the typical average annual offshore wind speed defined by IEC I wind class standard [4]. As an extreme example, the converters are subjected to 0.05 p.u. balanced grid voltage dips for 150 ms during the defined normal operation status. Studies of output pulses (green), load current (red), and grid voltage (blue) of each converter topology are presented in Fig. 9. It is obvious that, the current amplitude during LVRT with 0.05 p.u. grid voltage increases significantly in all of the three converter topologies compared to the normal operation with 10 m/s wind speed.

When zooming in the indicated areas of Fig. 9, the detailed output waveforms before and after LVRT are shown in Fig. 10. Compared to the normal operation with 10 m/s wind speed, the converter outputs when undergoing LVRT with 0.05 p.u. grid voltage have significant changes on the current amplitude, phase angle, and voltage pulse width. It can be seen that the load current lags the grid voltage 90 degree because of 100% reactive current injection, and the output voltage pulse width is largely reduced because of lower modulation index. It is noted that the output voltage level reduces from five to three in the 5L-HB topology when LVRT operation is presented.

The current distributions in the power switching devices of Fig. 10 are shown in Fig. 11. It is found that the current load moves from transistor to diodes (both freewheeling and

clamped diodes) in all of the three converter topologies during balanced LVRT, and the increased current amplitude will increase the stress of the power devices compared to the normal operation condition.

IV. LOSS DISTRIBUTION UNDER BALANCED LVRT

The power semiconductor switching devices play a crucial role in the loss, efficiency, reliability and cost of the converters for wind turbines. The dominant choices as reported in the wind power application are located in IGBT modules, IGBT press-pack and IGCT press-pack, which are generally compared in Table II [9].

Table II. Dominant power switching devices for wind power application.

	IGBT module	IGBT Press-pack	IGCT Press-pack
Power Density	Moderate	High	High
Reliability	Moderate	High	High
Cost	Moderate	High	High
Failure mode	Open circuit	Short circuit	Short circuit
Easy maintenance	+	-	-
Insulation of heat sink	+	-	-
Snubber requirement	-	-	+
Thermal resistance	Moderate	Small	Small
Switching loss	Low	Low	High
Conduction loss	High	High	Low
Gate driver	Small	Small	Large
Major manufacturers	Infineon, Mitsubishi ABB, Semikron, Fuji	Westcode, ABB	ABB
Medium voltage ratings	3.3 kV / 4.5 kV / 6.5kV	2.5 kV / 4.5 kV	4.5 kV / 6.5 kV
Max. current ratings	1.5 kV / 1.2 kA / 750 A	2.2 kA / 2.4 kA	2.1 kA / 1.3 kA

The module packaging technology for IGBT has longer record of applications and less mounting problems, however due to the soldering and bond-wire connection of chips, module packaging devices may suffer from larger thermal resistance, lower power density and higher failure rates [18]. The press-pack packaging technology improves the connection of chips by directly press-pack contacting, which leads to an increase in reliability (yet to be scientifically proven but known from industrial experience), higher power density (easier stacking for series connection) and better cooling capability at the disadvantage of higher cost compared to the module packaging devices.

Press-pack IGCT were introduced into the medium voltage converters in 90s and are already becoming state of the art in high power electric drives (e.g. for oil and gas application) but not yet widely adopted in the wind turbine industry also because of cost issues [18]-[20]. In this paper the press-pack IGCT 5SHY35L4512 (commutated voltage 2.8 kV/ maximum current 3.3 kArms) and diodes 5SDF16L4503 (2.8 kV/2.6 kArms) from ABB are chosen as the switching power devices for 3L-NPC and 3L-HB topologies, IGCT 5SHY35L4510 (2.8 kV/2.7 kArms) and diodes 5SDF10H4503 (2.8 kV/1.8 kArms) are chosen for the 5L-HB topology. The used loss model shares the same idea in [21],[22], which is a commonly accepted method for loss evaluation of power semiconductor devices, and the loss simulation is carried out based on PLECS Blockset in Simulink. Losses dissipated in the power devices are considered temperature independent during the simulation.

It is noted that during the LVRT operation, the DC bus of power converter may probably increase because of the short term mismatch in the input and output active power through the converter [7], [8]. Normally the increased DC bus voltage should be limited (e.g. maximum 110 % rated) for hundreds of milliseconds by triggering the braking chopper. According to the loss model in [22], the DC bus voltage has important impacts to both of the switching loss and the conduction loss in power switching devices. As a result, the increased DC bus voltage should be taken into account in the loss analysis during LVRT. Moreover, the increased DC bus voltage may significantly decrease the lifetime of power switching devices due to the cosmic radiation failure mechanism as reported in [18], however this issue will not be discussed this paper.

The loss distribution in the power switching devices under normal operation with wind speed of 8 m/s, 10 m/s, 12 m/s, as well as balanced LVRT condition with 0.05 p.u. grid
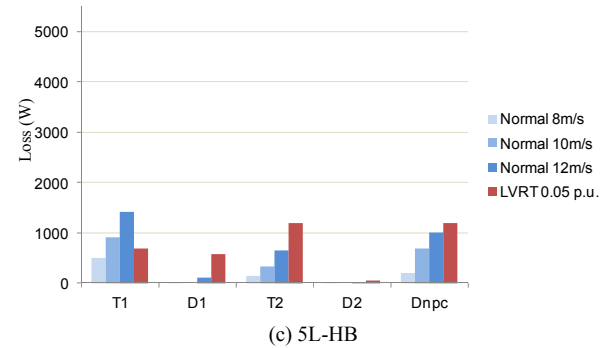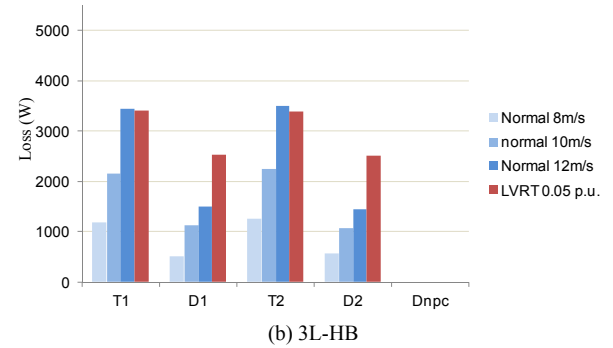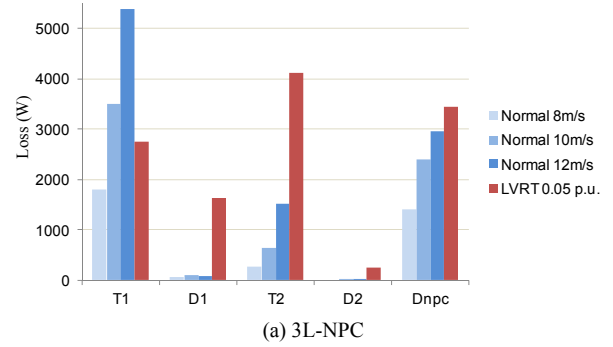

(a) 3L-NPC

(b) 3L-HB

(c) 5L-HB

Fig. 12. Loss distribution of converters under normal and balanced LVRT.

voltage are compared in Fig. 12, in which 10% higher DC bus voltage (3.1 kV or 6.2 kV) are applied for LVRT condition. It can be seen that, the LVRT operation may impose the diodes (D1, D2, Dnpc) and inner switches (T2 in 3L-NPC and 5L-HB) with significant larger losses than the most stressed normal operation condition (12 m/s wind speed, 10 MW rated output power). The loss simulation results are consistent with the current distributions in Fig. 11, in which the diodes and inner switches are heavy loaded because of increased current amplitude and moved phase angle between load current and grid voltage.

V. THERMAL DISTRIBUTION UNDER BALANCED LVRT

The thermal performance of power devices are closely related to the reliability of the converter, current rating of power devices and cost of the cooling system. Therefore it is an important indicator for large scale wind power converters. In order to conduct thermal performance evaluation, an appropriate thermal model should first be acquired.

The thermal models of a single switch and clamped diode are indicated in Fig. 13 [23], [24], in which the thermal impedance from junction to case $Z_{(j-c)}$ is modeled as a four-layers Foster RC network, as shown in Fig. 14. Each of the thermal parameters can be found from the manufacturer datasheets and they are summarized in Table III, where the thermal resistance R_{th} will decide the steady state mean value of the junction temperature, and the thermal capacitance (with time constant τ) will decide the dynamic change or fluctuation of the junction temperature. The ambient temperature is set to 50 ℃ and considered constant during the operation of converter. However it may be changed depends on the operation site.
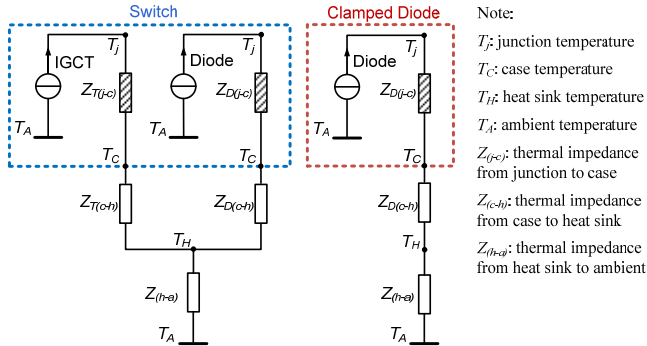

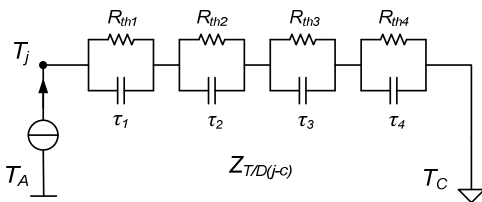Fig. 13. Thermal models of the power devices.

Fig. 14. Thermal model of the impedance $Z_{T(j-c)}$ or $Z_{D(j-c)}$ from junction to case in Fig. 13.

Table III. Parameters of thermal impedance for IGCT/diode.

Thermal Impedance	$Z_{T/D(j-c)}$				$Z_{T/D(c-h)}$
	Sector 1	Sector 2	Sector 3	Sector 4	
R_{iIGCT} (K/kW)	5.562	1.527	0.868	0.545	3
τ_{iIGCT} (s)	0.5119	0.896	0.0091	0.0024	-
R_{iDiode} (K/kW)	11.124	3.054	1.736	1.09	6
τ_{iDiode} (s)	0.5119	0.896	0.0091	0.0024	-

It is noted that the separately packaged IGCT and diodes are chosen because of the limitation for available products which can be found on the market. However, in a practical converter design, the IGCT/IGBT and its freewheeling diode are usually integrated and packaged together, the chip size for diode is usually about half of that for the IGCT/IGBT, accordingly, the thermal resistance of the diode from junction to heat sink is not consistent with its datasheet but set to twice of the IGCT.

Normally, the thermal capacitance outside a power device from case to ambient are much larger compared to that inside a power device from junction to case in a properly designed cooling system. The larger thermal capacitance, which has longer time constant ranging from hundreds of milliseconds to hundreds of seconds [25], mostly decide the time to achieve steady-state junction temperature, and have no significant impacts on the dynamic junction temperature fluctuation within a fundamental cycle of the converter output (dozens of milliseconds). Therefore it is efficient to make a simplification which ignores the relative larger thermal capacitances in $Z_{(c-h)}$ and $Z_{(h-a)}$ to realize a faster thermal simulation. In mega-watts power converter systems, separated heat sink is typically used, a good thermal decoupling among the power devices can be achieved, so the thermal resistance between the heat sink and ambient is considered small.

Based on the previous loss simulation results and thermal model, the junction temperature of the power devices in each of the converter solution can be investigated by the PLECS blockset in Simulink.

A. 3L-NPC

The simulated junction temperature in 3L-NPC converter under normal operation with 10 m/s wind speed and three-phase balanced LVRT condition with 0.05 p.u. grid voltage are shown in Fig. 15. It can be seen that the thermal distribution is quite unequal under both operation modes. The LVRT operation has higher junction temperate in all of the switching devices except the outer switch T1, and the maximum temperature which locates in the clamped diode D_{npc} increases about 20 K compared to the normal operation at 10 m/s wind speed.
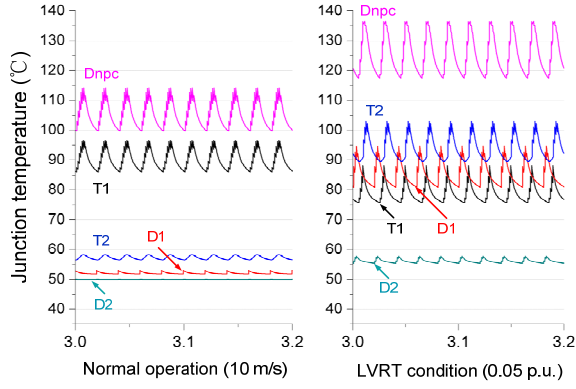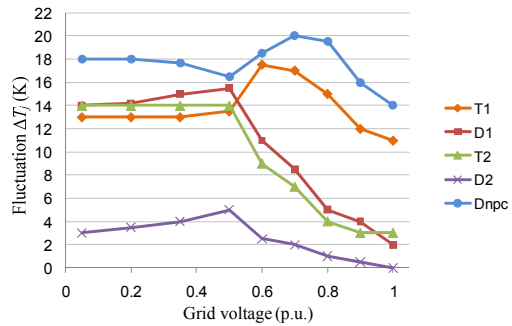
Fig. 15. Junction temperature in normal operation vs. LVRT in 3L-NPC converter (normal operation: v_w=10 m/s, P_G=6.3 MW / LVRT: V_g=0.05 p.u.).

According to the important Coffin-Masson life time model [24], [25], the junction temperature mean value T_m and the fluctuation amplitude ΔT_j, are two of the most important information for the reliability of power semiconductor devices, the simulated T_m and ΔT_j of each switching device in 3L-NPC converter with relation to the grid voltage are shown in Fig. 16 (a) and Fig. 16 (b) respectively. The change of junction temperature keeps relative smooth when the grid voltage is below 0.5 p.u., and becomes dramatic when the grid voltage is above 0.5 p.u.. It is noted that there is a temperature rise in Dnpc and T1 when the grid voltage is around 0.7 p.u., which is due to the current phase angle change and the fast growing switching loss in T1 and Dnpc.
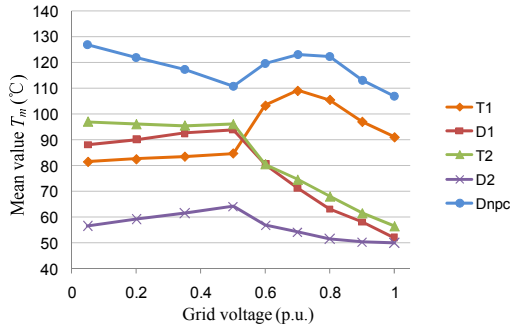
(a) Junction temperature mean value T_m vs. grid voltage.

(b) Junction temperature fluctuation ΔT_j vs. grid voltage.

Fig. 16. Junction temperature distribution under balanced LVRT in 3L-NPC converter (v_w=10 m/s).

B. 3L-HB

The simulated junction temperature in 3L-HB converter under normal operation with 10 m/s wind speed and LVRT condition with 0.05 p.u. grid voltage are compared in Fig. 17. It can be seen that the junction temperature is equally distributed among all of the switching devices under normal operation, and significantly increases especially in the diodes under LVRT. The maximum temperature which is located in
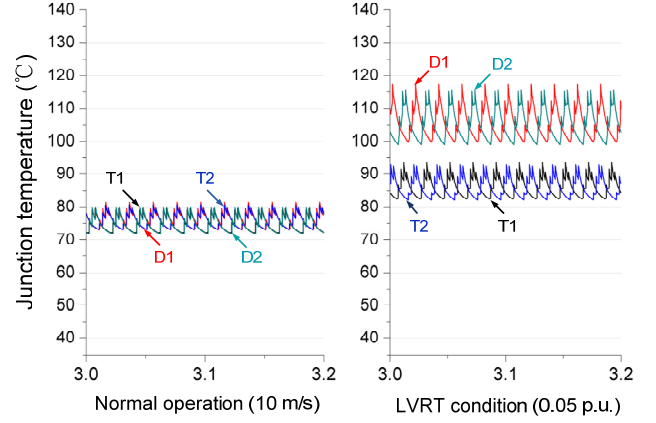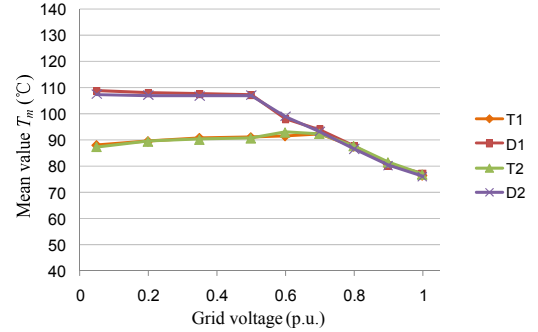

Fig. 17. Junction temperature in normal operation vs. LVRT in 3L-HB converter (simulation results, normal operation: v_w=10 m/s, P_G=6.3 MW / LVRT: V_g=0.05 p.u., $I_{reactive}$=100% I_{rated}).

(a) Junction temperature mean value T_m vs. grid voltage p.u.

(b) Junction temperature fluctuation ΔT_j vs. grid voltage p.u.

Fig. 18. Junction temperature distribution under balanced LVRT in 3L-HB converter (v_w=10 m/s).

the freewheeling diodes D1/D2 increases about 35 K compared to the normal operation with 10 m/s wind speed.

The simulated temperatures T_m and ΔT_j in 3L-HB converter with relation to the grid voltage are shown in Fig. 18. It is interesting to see that the thermal distribution in 3L-HB topology under LVRT is much more equal than the 3L-NPC in Fig. 16, and both of the junction temperature mean value and amplitude keep reducing when the grid voltage is above 0.5 p.u..

C. 5L-HB

The junction temperature in the 5L-HB converter under normal operation with 10 m/s wind speed and LVRT condition with 0.05 p.u. grid voltage are compared in Fig. 19, and the simulated T_m and ΔT_j in 5L-HB converter with relation to the grid voltage are shown in Fig. 20.

It can be seen that the trends of thermal performance in the 5L-HB topology under LVRT is quite similar to that of the 3L-NPC topology, but the junction temperature keeps at a much lower level. This is because of the half current rating compared to the 3L-NPC topology.
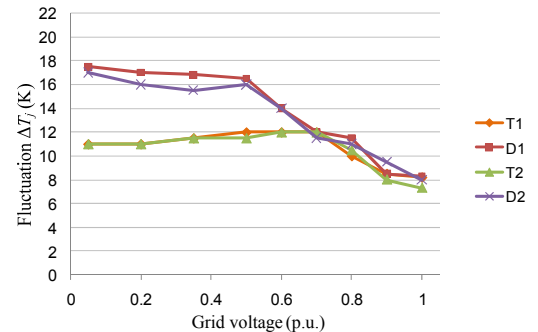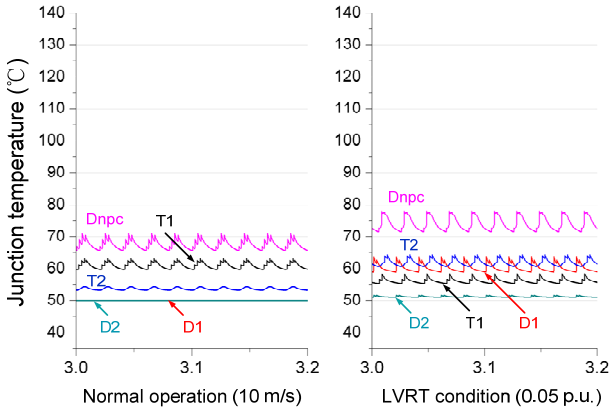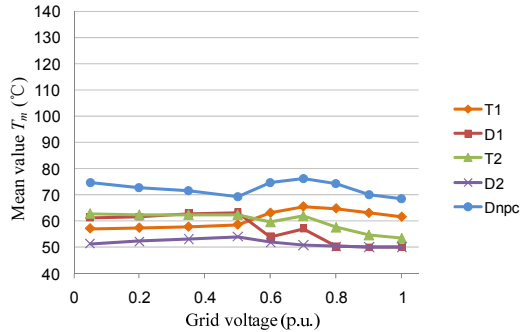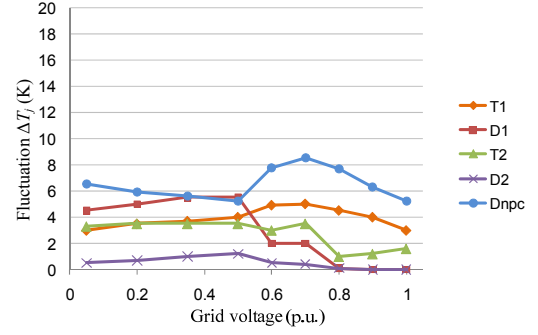

Fig. 19. Junction temperature in normal operation vs. LVRT in 5L-HB converter (simulation results, normal operation: v_w=10 m/s, P_G=6.3 MW / LVRT: V_g=0.05 p.u., $I_{reactive}$=100% I_{rated}).

(a) Junction temperature mean value T_m　vs. grid voltage p.u.

(b) Junction temperature fluctuation ΔT_j　vs. grid voltage p.u.

Fig. 20. Junction temperature distribution under balanced LVRT in 5L-HB converter (v_w=10 m/s).

D. Comparison of topologies

The junction temperature comparison of the most stressed power device in each of the converter topology is shown in Fig. 21, in which the fluctuation range of the junction temperature is indicated. It can be seen that the 3L-NPC converter has the most stressed switching devices Dnpc among the three converter topologies, and the most extreme condition happens when the grid voltage is close to 0 p.u. (due to the large conduction losses) and 0.7 p.u. (due to the large switching losses). For the 3L-HB topology, it has a better thermal performance compared to the 3L-NPC topology, especially when the grid voltage is above 0.5 p.u.. The 5L-HB shows the best temperature performance among the three topologies, and shares the similar junction temperature changing trends as 3L-NPC converter. This also means that it has more potential to handle higher power or reduce the cost for cooling system and power semiconductors.
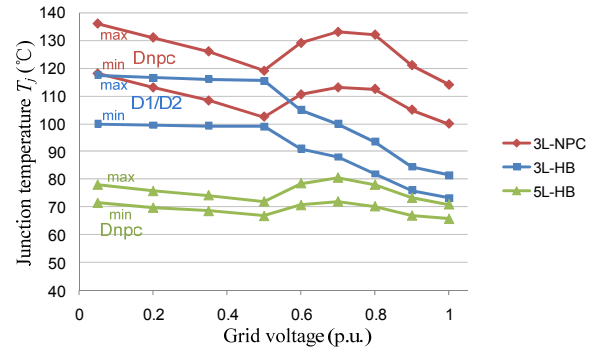
Fig. 21. Junction temperature comparison between converters under balanced LVRT (10 m/s, most stressed device).

VI. UNBALANCED LVRT

In reality the unbalanced grid faults (e.g. one-phase grounded or two-phase connected) are more likely to happen. In these cases the LVRT operation of the grid side converter is more complicated compared to the balanced fault condition (three-phase grounded). During the unbalanced LVRT, the types and location of grid faults, the connection of

transformer windings and the power control strategies of the converter all dramatically change the loading of power switching devices. Therefore the operation conditions for unbalanced grid fault have to be carefully specified.

A. Propagation of Voltage Dips

A typical configuration for grid integration of wind turbine is shown in Fig. 22, in which a Dy transformer is used to interface the power converter output on Bus 2 (e.g. 3.3 kV) and the distribution line of wind farm on Bus 1 (e.g. 20 kV). A short circuit fault in the grid integration system will cause voltage dips on Bus 1 and Bus 2.
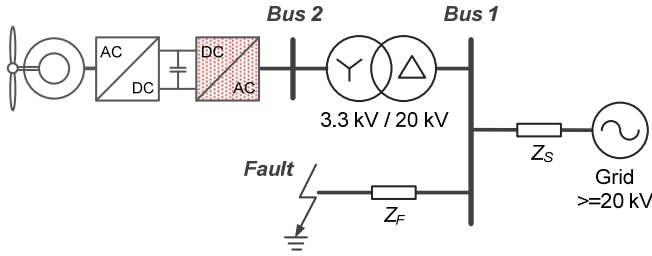

Fig. 22. Typical configuration for grid integration of wind power generation system.

Define that the voltage dip value D_N represents the lowest phase voltage amplitude in p.u. on the Bus N. Three typical grid faults: one-phase grounded (1 phase), two-phase connected (2 phase) and three-phase grounded (3 phase) with the same dip value are assumed to happen respectively on Bus 1 (D_1=0.5, no phase jump). Due to the Dy connection of the transformer windings, the voltage dips propagated from Bus 1 may look different on Bus 2 [26]. As summarized in Table IV, in which the voltage dip type and dip value on Bus 1 and the corresponding voltage characteristics on Bus 2 are included. The voltage dip types A-D are defined as phasor diagrams in Fig. 23 respectively [26], [28].

Table IV. Voltage dip type/value on Bus 1 and Bus 2 for different grid faults.

Fault type		1 phase	2 phase	3 phase
Bus1	Dip type	B	C	A
	Dip value D_1 (p.u.)	0.5	0.5	0.5
Bus2	Dip type	C	D	A
	Dip value D_2 (p.u.)	0.76	0	0.5
	Positive sequence V^+ (p.u.)	0.83	0.5	0.5
	Negative sequence V^- (p.u.)	0.17	-0.5	0

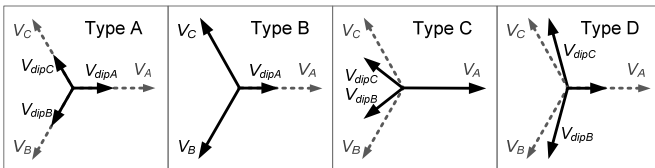Note: Two-phase grounded fault is not included because it seldom happens.

Fig. 23. Phasor diagram definitions for the dip types A-D.

It can be seen that the three-phase balanced grid fault (3 phase) on Bus 1 propagates the same dip type and dip value on Bus 2. While the unbalanced grid faults (1 phase and 2 phase) with the same dip value on Bus 1 cause different dip types and dip values on Bus 2, which is monitored by the grid side converter and result in different amount of delivered reactive currents to help the grid to recover from faults.

The whole range of voltage dip value on Bus 1 with ralation to the coresponding dip value on Bus 2 are shown in Fig. 24, in which balanced (3 phase) and unbalanced (1 phase and 2 phase) grid faults are indicated respectively. It is clear that the balanced grid fault on Bus 1 will propogate the same dip value on Bus 2. While the single-phase unbalanced grid fault happened on Bus 1 has a higher dip value when propogating on Bus 2, and the two-phase unbalanced grid fault on Bus 1 has lower dip value when propagating on Bus 2.
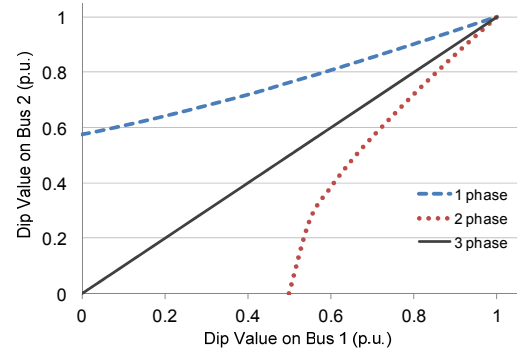

Fig. 24. Dip value on Bus 2 vs. dip value on Bus 1.

For simplicity of the analysis only the single-phase grounded faults on Bus 1 is chosen in this paper as an example of the unbalanced LVRT. The injected reactive current to the grid by wind power converter is set according to the lowest phase voltage amplitude on Bus 2 referring to the demands in Fig. 2. It is required that the active/reactive current generated by the converters only contains positive sequence component, and the negative sequence currents are controlled to be zero. The control methods for different sequence currents can be found in [27], and the behavior of converters under various LVRT is still a continuous discussion for the future grid standards.

B. Operation Status under Single-phase Unbalanced Grid Fault

The active/reactive power delivered by the grid side converter under single phase unbalanced grid voltage dip is shown in Fig. 25, where the horizontal axis represents the voltage dip values on Bus 2. It is noted that the single-phase voltage dip on Bus 1 (type B) propagates two-phase voltage dip on Bus 2 (type C), whose dip value D_2 can not be lower than 0.577 due to the characteristic of Dy transformer. The situations of 12 m/s wind speed (10 MW generated power), 10 m/s (6.3 MW generated power) and 8 m/s (3.2 MW generated power) are indicated respectively.
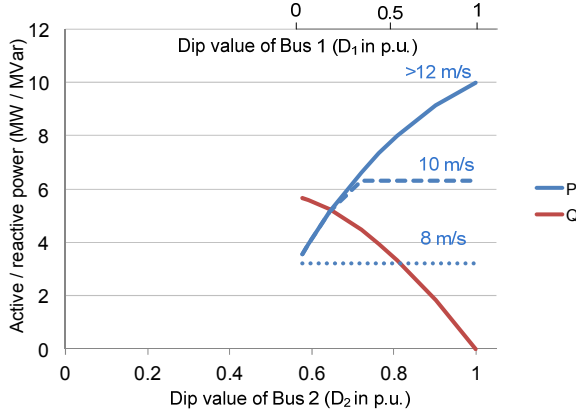
Fig. 25. Active and reactive power delivered by converter during single phase grid fault (based on German grid codes in Fig. 2).
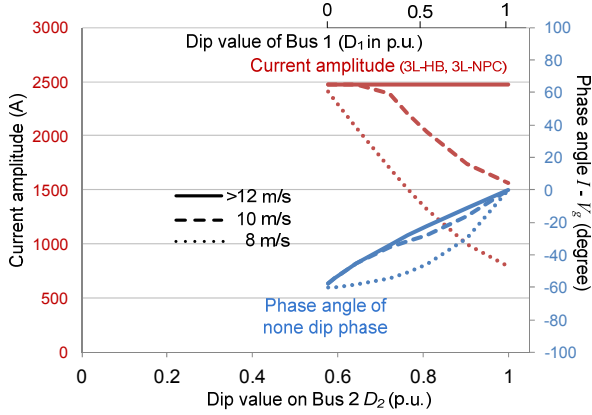

Fig. 26. Positive sequence amplitude and phase angle of the load current during single phase grid fault (based on German grid codes in Fig. 2, 5L-HB has half the current amplitude).

The current amplitude as well as the phase angle under single-phase unbalanced grid fault is shown in Fig. 26, where the phase angle represents the angle between the load current and grid voltage of A phase in the type C grid fault definition diagram (Fig. 23). It can be seen that the current amplitude and phase angle dramatically change with the variation of grid voltage and wind speed.

As an example, Fig. 27 shows the grid voltage, load current as well as instantaneous active/reactive power of wind power converter undergoing single-phase unbalanced grid fault on Bus 1. The wind speed is at 10 m/s (6.3 MW), the dip value D_1 is at 0 p.u. (0.577 p.u. when propagated to Bus 2), the positive sequence active current is at 0.533 p.u. and the reactive current is at 0.864 p.u. according to the grid codes in Fig. 2.

It can be seen that the grid voltage on Bus 2 is consistent with the type C fault definition in Fig. 23, and the currents in the converter are symmetrical among three phases, that means only positive sequence currents are generated. Due to the existing of negative sequence voltage, there is a 100 Hz fluctuation in the delivered active and reactive power of converter [25], [28] which is assumed to be absorbed by the DC bus chopper.
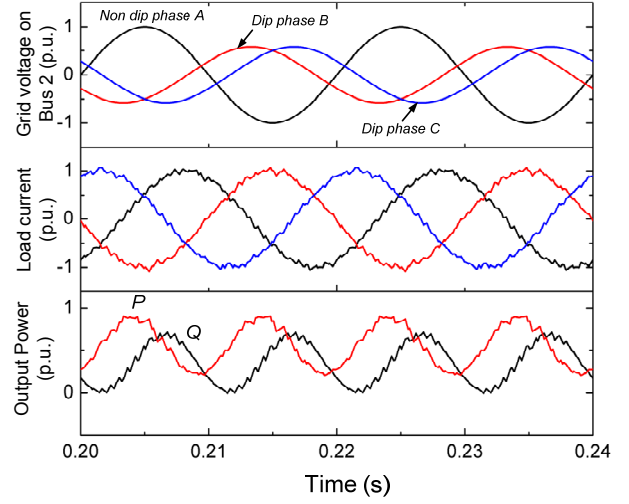

Fig. 27. Output waveforms during unbalanced grid fault. (Type C fault on Bus 2 with D_2=0.577 p.u., v_w=10 m/s)
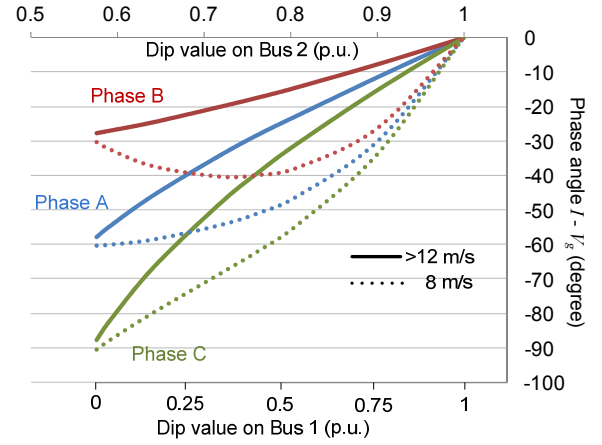

Fig. 28. Phase angle (load current to grid voltage) for three phases of the power converter (Type C fault on Bus 2).

By looking at the phasor diagram definition for grid voltage dip type C in Fig. 23, it is interesting to see that when the single-phase grid fault is presented on Bus 1, there is a phase shift in the voltage of phase B and C on Bus 2, and thereby the angle between each phase voltage is no longer 120 degree. On the other hand it is required that only positive sequence currents should be delivered by the wind power converter, therefore the angle between each phase current is still kept at 120 degree, as shown in Fig. 27.

Fig. 28 shows the phase angles (between phase voltage and current) for the three phases of wind power converter with relation to the voltage dips when single-phase unbalanced grid fault is presented. The conditions with wind speeds of 12 m/s and 8 m/s are indicated respectively.

As mentioned before, the phase angles as well as the voltage/current amplitude are closely related to the loading of power switching devices. By Fig. 27 and Fig. 28 it can be seen that the voltage amplitude and phase angle of the three

phases of the converter are quite different from each other, therefore, the device losses and thermal distribution should also be different for each phase of the converter when undergoing unbalanced LVRT.

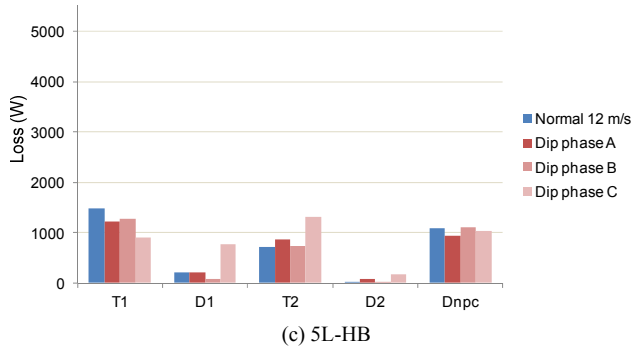### C. Loss Analysis under Single-phase Unbalance Grid Fault

The loss distribution of the power switching devices under normal operation (with wind speed of 12 m/s), and the loss distribution for the three phases of converters under unbalanced LVRT, are compared in Fig. 29. The 10% higher DC bus voltage is applied for LVRT condition. It can be seen that, the LVRT operation still impose the diodes and inner switches with significant larger losses than the most stressed normal operation condition, and the loss distribution among the three phases are asymmetrical for each topology.
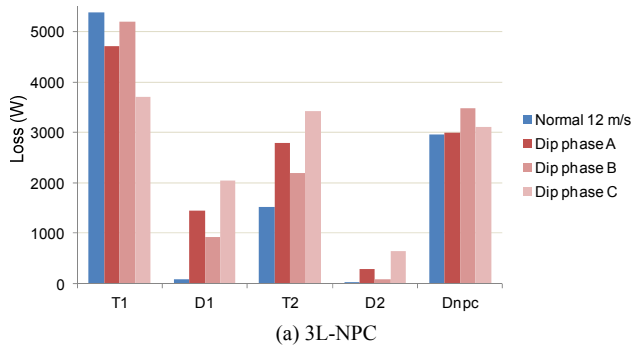
(a) 3L-NPC
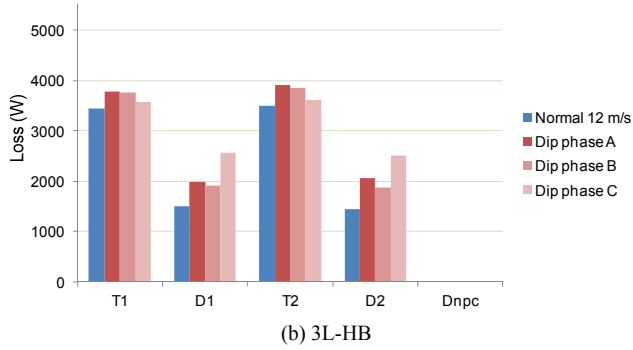
(b) 3L-HB

(c) 5L-HB

Fig. 29. Loss distribution of converters under normal and unbalanced LVRT. (Type C fault on Bus 2 with D_2=0.577 p.u., v_w=10 m/s)

D. Thermal Distribution under Single-phase Unbalanced Grid Fault
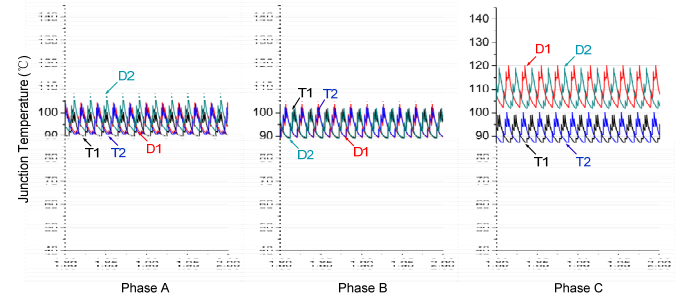
The simulated junction temperatures for the three phases

of converters are shown in Fig. 30, in which the converters are undergoing unbalanced LVRT (Type C fault on Bus 2 with D_2=0.577 p.u., v_w=10 m/s). It can be seen that for the 3L-NPC topology, the thermal distribution is unequal not only among the devices but also among the three phases. Phase B has a more stressed D_{npc} and T_1 while phase A and phase C have more stressed T_2, D_1 and D_2. It is found that D_{npc} in phase B is the most stressed device of the converter under the given condition.

For the 3L-HB topology, the thermal distribution is much more equal both among the devices and the three phases, D_1/D_2 in phase C is the most stressed devices of the converter.

For the 5L-HB converter, thermal distribution tendency is similar to the 3L-NPC topology, but the inequity among the devices and the three phases are significantly improved.
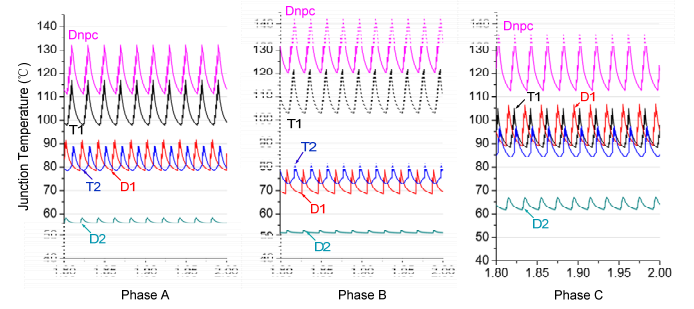
(a) 3L-NPC

(b) 3L-HB
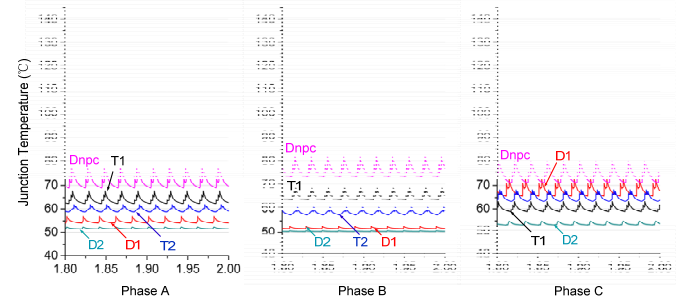
(c) 5L-HB

Fig. 30. Thermal distribution in three phases of converters under unbalanced LVRT. (Type C fault on Bus 2 with D_2=0.577 p.u., v_w=10 m/s)

The junction temperature comparison of the most stressed power device among the three phases in each of the converter topology is shown in Fig. 31, in which the fluctuation range of the junction temperature is indicated. Again 3L-HB and

5L-HB topologies show advantages under unbalanced LVRT condition (Type C fault on Bus 2, v_w=10 m/s).

Fig. 31. Junction temperature comparison between converters under unbalanced LVRT (most stressed device in three phases, Type C fault on Bus 2, v_w=10 m/s).
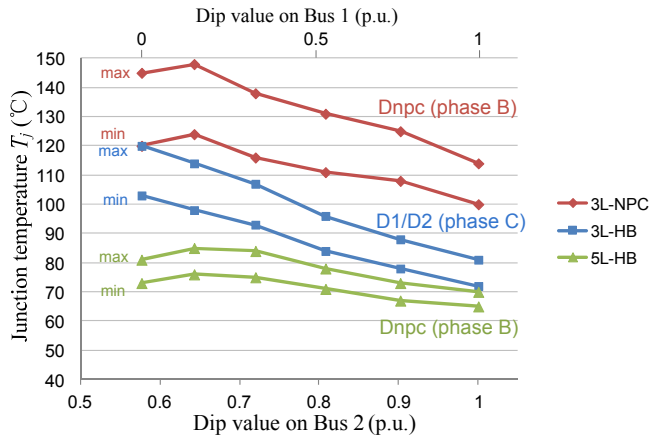
VII. CONCLUSION

The reactive current injection requirements for full scale wind power converter during LVRT will impose some power switching devices (especially the diodes) with even larger stress than the rated normal operation condition.

The device loading of the grid side converter under balanced LVRT changes dramatically under different grid voltage dips. When the grid voltage is below 0.5 p.u., 100% rated reactive current is needed, the amplitude and position of the current keeps fixed and only the conduction loss is changed in the power devices. While when the grid voltage is above 0.5 p.u., both switching loss and conduction loss are changed dramatically in the power devices because the grid code allows some room and flexibility for the active current, which is related to the wind speed as well as the pitch angle/rotation speed control strategies for wind turbines during LVRT.

When undergoing single phase unbalanced grid fault, it is found that the device loading among the three phases of converter is asymmetrical for all of the interested topologies. And it is also found that both of the three-level and five-level H-bridge topologies show more potential to reduce and more equally distribute the stress in the power switching devices compared to the well-known three-level Neutral Point Clamped topology under various LVRT conditions.

REFERENCES

[1] European Commission Climate Action, "The EU climate and energy package", March 2007.
[2] F. Blaabjerg, Z. Chen, S.B. Kjaer, "Power Electronics as Efficient Interface in Dispersed Power Generation Systems", *IEEE Transactions on Power Electronics*, 2004, vol. 19, no. 4, pp. 1184-1194.
[3] Z. Chen, J.M. Guerrero, F. Blaabjerg, "A Review of the State of the Art of Power Electronics for Wind Turbines," *IEEE Transactions on Power Electronics,* vol.24, no.8, pp.1859-1875, Aug. 2009.
[4] Website of Vestas Wind Power, Wind turbines overview, April 2011. (Available: http://www.vestas.com/)
[5] M. Altin, O. Goksu, R. Teodorescu, P. Rodriguez, B. Bak-Jensen, L. Helle, "Overview of recent grid codes for wind power integration," Proc. of OPTIM'2010, pp.1152-1160, 2010.
[6] E.ON-Netz – Grid Code. High and extra high voltage, April 2006.
[7] S.M.Muyeen, R.Takahashi, T.Murata, J.Tamura, "A Variable Speed Wind Turbine Control Strategy to Meet Wind Farm Grid Code Requirements," *IEEE Transactions on Power Systems*, 2010, vol. 25, no. 1, pp. 331-340.
[8] S. Alepuz, S. Busquets-Monge, J. Bordonau, J.A. Martinez-Velasco, C.A. Silva, J. Pontt, J. Rodriguez, "Control Strategies Based on Symmetrical Components for Grid-Connected Converters Under Voltage Dips," *IEEE Transactions on Industrial Electronics,* vol. 56, no. 6, pp. 2162-2173, 2009.
[9] F. Blaabjerg, M. Liserre, K. Ma, "Power Electronics Converters for Wind Turbine Systems," *IEEE Transactions on Industrial Application,* 2012.
[10] S. Kouro, M. Malinowski, K. Gopakumar, J. Pou, L. G. Franquelo, B. Wu, J. Rodriguez, M. A. Perez, J. I. Leon, "Recent Advances and Industrial Applications of Multilevel Converters," *IEEE Transactions on Power Electronics*, vol. 57, no. 8, pp. 2553 – 2580, 2010.
[11] K. Ma, F. Blaabjerg, D. Xu, "Power Devices Loading in Multilevel Converters for 10 MW Wind Turbines," in *Proc. of ISIE*, pp. 340-346, June 2011.
[12] K. Ma, F. Blaabjerg, "Multilevel Converters for 10 MW Wind Turbines," in *Proc. of EPE*, August 2011.
[13] O. S. Senturk, L. Helle, S. Munk-Nielsen, P. Rodriguez, R. Teodorescu, "Medium voltage three-level converters for the grid connection of a multi-MW wind turbine," in *Proc. of EPE'09*, pp: 1- 8, 2009.
[14] J. Holtz, N. Oikonomou, "Optimal Control of a Dual Three-Level Inverter System for Medium-Voltage Drives," *IEEE Transactions on Industrial Applications,* vol. 46, no. 3, pp. 1034-1041, 2010.
[15] H. Hosoda, S. Peak, "Multi-level converters for large capacity motor drive," in *Proc. of IECON'10*, pp. 516-522, 2010.
[16] H. Li, Z. Chen, H. Polinder, "Optimization of Multibrid Permanent-Magnet Wind Generator Systems," *IEEE Transactions on Energy Conversion,* vol. 24, no. 1, pp. 82-92, 2009.
[17] H.Polinder, F.F.A.van der Pijl, G.-J.de Vilder, P.J.Tavner, "Comparison of direct-drive and geared generator concepts for wind turbines," *IEEE Transactions on Energy Conversion,* vol. 21, no. 3, pp. 725-733, 2006.
[18] C. Busca, R. Teodorescu, F. Blaabjerg, S. Munk-Nielsen, L. Helle, T. Abeyasekera, P. Rodriguez, "An overview of the reliability prediction related aspects of high power IGBTs in wind power applications," Microelectronics Reliability, Vol. 51, no. 9-11, September-November 2011, pp. 1903-1907.
[19] R. Jakob, C. Keller, B. Gollentz, "3-Level high power converter with press pack IGBT," in Proc. EPE 2007, 2-5 Sept. 2007.
[20] Rodrigo Alvarez, Felipe Filsecker, Steffen Bernet, "Comparison of press-pack IGBT at hard switching and clamp operation for medium voltage converters," in Proc. EPE 2011, 2011.
[21] User manual of PLECS blockset version 3.1, March 2011. (Available: http://www.plexim.com/files/plecsmanual.pdf).
[22] F. Blaabjerg, U. Jaeger, S. Munk-Nielsen and J. Pedersen, "Power Losses in PWM-VSI Inverter Using NPT or PT IGBT Devices," *IEEE Transactions on Power Electronics,* vol. 10, no. 3, pp. 358–367, May 1995.
[23] ABB Application Note: Applying IGBTs, May 2007.
[24] W. Lixiang, J. McGuire,R.A. Lukaszewski, "Analysis of PWM Frequency Control to Improve the Lifetime of PWM Inverter," *IEEE Transactions on Industrial Electronics,* vol. 47, no. 2, pp. 922-929, 2011.

[25] I.F. Kovačević, U. Drofenik, J.W. Kolar, "New physical model for lifetime estimation of power modules," in *Proc.of IPEC'10*, pp. 2106-2114, 2010.

[26] G. Saccomando, J. Svensson, A. Sannino, "Improving voltage disturbance rejection for variable-speed wind turbines," *IEEE Transactions on Energy Conversion,* vol. 17, no. 3, pp. 422-428, 2002.

[27] P. Rodriguez, A.V. Timbus, R. Teodorescu, M. Liserre, F. Blaabjerg, "Flexible Active Power Control of Distributed Power Generation Systems During Grid Faults," *IEEE Transactions on Industrial Electronics,* vol. 54, no. 5, pp. 2583-2592, 2007.

[28] C.H. Ng,Li Ran; J. Bumby, "Unbalanced-Grid-Fault Ride-Through Control for a Wind Turbine Inverter," *IEEE Transactions on Industry Applications,* vol. 44, no. 3, pp. 845-856, 2008.